Understanding the monoclonal antibody disposition after subcutaneous administration using a minimal physiologically based pharmacokinetic model

Ninad Varkhede[1], M. Laird Forrest[1,2]

[1]Department of Pharmaceutical Chemistry, The University of Kansas, Lawrence, Kansas 66047, USA

[2]To whom correspondence should be addressed. (2095 Constant Ave Lawrence, KS 66047; Telephone: 785-864-4388; e-mail: lforrest@ku.edu)

ABSTRACT

Purpose: Monoclonal antibodies (mAbs) are commonly administered by subcutaneous (SC) route. However, bioavailability is often reduced after SC administration. In addition, the sequential transfer of mAbs through the SC tissue and lymphatic system is not completely understood. Therefore, major objectives of this study were a) To understand absorption of mAbs via the lymphatic system after SC administration using physiologically based pharmacokinetic (PBPK) modeling, and b) to demonstrate application of the model for prediction of SC pharmacokinetics (PK) of mAbs.

Methods: A minimal PBPK model was constructed using various physiological parameters related to the SC injection site and lymphatic system. The remainder of the body organs were represented using a 2-compartment model (central and peripheral compartments), with parameters derived from available intravenous (IV) PK data. The IV and SC clinical PK data of a total of 10 mAbs were obtained from literature. The SC PK data were used to estimate the lymphatic trunk-lymph node (LN) clearance.

Results: The mean estimated lymphatic trunk-LN clearance obtained from 37 SC PK profiles of mAbs was 0.00213 L/h (0.001332 to 0.002928, 95% confidence intervals). The estimated lymphatic trunk-LN

clearance was greater for the mAbs with higher isoelectric point (*pI*). In addition, the estimated clearance increased with decrease in the bioavailability.

Conclusion: The minimal PBPK model identified SC injection site lymph flow, afferent and efferent lymph flows, and volumes associated with the SC injection site, lymphatic capillaries and lymphatic trunk-LN as important physiological parameters governing the absorption of mAbs after SC administration. The model may be used to predict PK of mAbs using the relationship of lymphatic trunk-LN clearance and the *pI*. In addition, the model can be used as a bottom platform to incorporate SC and lymphatic *in vitro* clearance data for mAb PK prediction in the future.

KEYWORDS

Physiologically based pharmacokinetic model, monoclonal antibody, subcutaneous, proteolysis, lymph flow, lymph node, lymphatic system

INTRODUCTION

Monoclonal antibodies (mAbs) are an important class of therapeutic proteins (TPs) administered mainly via subcutaneous (SC) route due to shorter clinical visits for patients, the possibility of self-administration, and its less invasive nature. However, when compared to the intravenous (IV) route, SC injection has challenges associated with the incomplete bioavailability and pain-free administration of larger fluid volumes (1). The SC tissue and lymphatic system are important barriers for the absorption of mAbs. After SC administration, the mAbs travel through the lymphatic vessels and lymph nodes before reaching the systemic circulation. The SC bioavailability of mAbs is typically in the range of 52 to 80% (2, 3). Proteolysis within the lymphatic system and the SC injection site may be partially responsible for the reduced bioavailability of mAbs. The rate of neonatal Fc receptor (FcRn) binding and recycling exceeds

the rate of lysosomal/endosomal trafficking of mAbs; therefore, endosomal proteolysis may contribute only minimally to low mAb bioavailability (3, 4). In addition, the target mediated drug disposition (TMDD) is often saturated due to limited receptors. Thus, mAbs are cleared slowly from the systemic circulation. The TPs like IgG1, IgG2 and IgG4 have a long half-life of around 23 days (3), which is substantially longer than other proteins of similar molecular weights. Further, the appearance rate of mAbs in the plasma is slow (T_{max} generally 2-14 days) (3). The low bioavailability of mAbs may result from efficient pre-systemic clearance mechanisms or irreversible retention (and subsequent elimination) of significant dose at the injection site or in the surrounding tissues.

Charman et al. investigated the causes of reduced bioavailability of human growth hormone (hGH) protein using a sheep model. The SC injection site degradation was minimal for hGH, while the lymphatic proteolysis was mainly responsible for its reduced bioavailability after SC administration (5). We hypothesize that the interstitial proteolysis in the lymphatic system may be responsible for lower bioavailability of mAbs after SC administration. In this study, a minimal physiologically based pharmacokinetic (PBPK) model was used to understand the sequential transit of mAbs and to estimate lymphatic clearance using the SC pharmacokinetics (PK). The model was constructed using physiological parameters related to the SC injection site, lymphatic system and the reported clinical IV PK data. This study had the following major objectives: a) construction of the minimal PBPK model focusing on the lymphatic transit of mAbs after SC administration using physiologically relevant lymph flows and compartment volumes, b) estimation of the lymphatic clearance using literature SC PK data, and c) identification of the parameters governing the absorption of mAbs via the SC and lymphatic system.

Various PBPK models for TPs have been reported recently and as early as 1995 (Gill et al., Abbuqayyas and Balthasar, Garg and Balthasar, Baxter et al., Shah and Betts) (6-9). Some of the authors (Zhao et al., Chen et al., Elmeliegy et al., Li et al.) proposed the minimal PBPK approach to eliminate complexity associated with the models (3, 10-12). Although, these models may be useful for a mechanistic

understanding of the clearance and absorption processes at the SC injection site and in the lymphatic system, use of PBPK modeling for TP PK prediction is limited (13). After SC injection, the mAb travels through the lymphatic capillary network, lymph nodes, lymphatic trunks and thoracic lymph duct before joining the systemic circulation. Hence, in this study, the lymphatic organs were incorporated in the minimal PBPK model, and the lymphatic trunk-lymph node (LN) clearance was estimated using the SC PK. Interestingly, it appears that the estimated lymphatic trunk-LN clearance was directly proportional to the isoelectric point (*pI*) of the mAb. In addition, the model must be combined in the future with *in vitro* proteolysis data obtained from the lymphatic system to predict SC PK and bioavailability of mAbs. Further, the variability in the PK due to different populations, disease conditions, formulations, novel delivery technologies, and biophysical properties of the TP may be addressed using the minimal PBPK model (14). Overall, the proposed minimal PBPK model can be used for mechanistic understanding mAb absorption and prediction of PK after SC administration.

METHODS

Digitization of literature IV and SC PK data

The IV (35 profiles) and SC (37 profiles) PK of 10 mAbs were obtained from literature and digitized using WebPlotDigitizer (version 4.1) (15). This web-based tool has been extensively used in other reports (16). The IV PK profiles were used to estimate 2-compartment model parameters, while the SC PK profiles were used to estimate the lymphatic trunk-LNs clearance.

Construction of the minimal PBPK model

The minimal PBPK model was constructed using SimBiology (Matlab R2017a). The physiologically based model and simple compartmental model were combined to describe absorption of mAbs after SC administration (Figure 1). The model equations describing FcRn binding and transfer across interstitial, endosomal and vascular space were adopted from previously reported studies (3, 9, 17). However, additional physiological parameters related to the lymphatic system were either calculated or obtained from

the literature (Table 1) and used to construct the model. The model parameters specific to mAbs are listed in Table 2. Furthermore, additional compartments were included to describe the sequential transfer of mAbs through the lymphatic system. It was assumed that the SC dose of mAb distributes equally in the SC interstitial space after the injection.

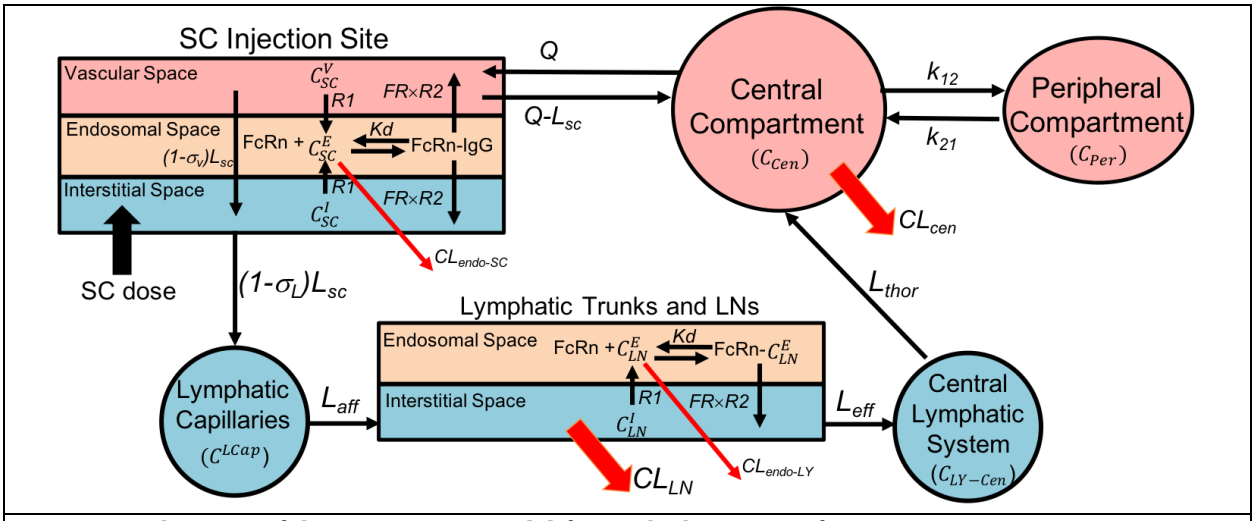

Figure 1: Schematic of the semi-PBPK model for mAb absorption after SC injection

Physiological parameters related to the SC injection site and lymphatic system

The physiological parameters related to the SC injection site and lymphatic system were either obtained or calculated from the literature (Table 1). The SC injection site volume was calculated by Gill et al. (9) using the diameter of the SC injection depot of radiolabeled IgG. While, the SC site lymph flow was measured using the rate of radiolabeled IgG loss from a SC administration site (9). Lymphatic capillary volume was calculated using the average distance between the injection site and sentinel LN (30 cm), the lymphatic network density per 1 cm annulus of arm skin (385 cm), and the average radius of lymphatic capillaries (0.0274 mm) (18-20). Afferent lymph flow was calculated using the reported lymphatic flow rate (40 mm/min) and radius (0.0274 mm) of the lymphatic capillaries in humans (21, 22). The efferent lymph flow rate in sheep was used in the model (23). The volume of the lymphatic trunk was calculated based on an approximate length of 30 cm and a radius of 1 mm (20).

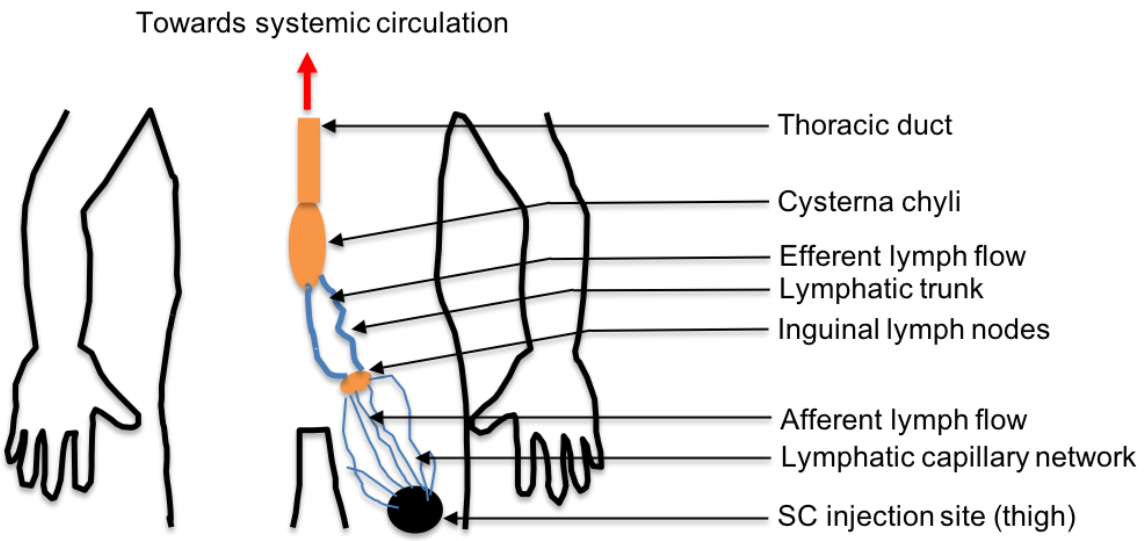

Figure 2: Schematic representation of flow of mAbs or TPs after SC injection in thigh

The total LNs volume was calculated based on the number of LNs (45 to 50) to which the mAb is exposed after SC injection in thigh (24-26). The average volume of cervical LNs (0.292 mL) reported in humans was used to calculate the total LN volume after SC injection in the upper arm, abdomen, and thigh (27). The SC injection of a TP in thigh would lead to its travel through the inguinal, iliac and lumbar LNs (Figure 2). Upon SC injection in the upper arm, the TP would travel through the cubital and axillary LNs followed by the subclavian trunk. After passing through the LNs and lymphatic trunks, TPs would join the central lymphatic system (thoracic duct and cysterna chyli), which are lymphatic vessels with greater diameters. The TP would join the systemic circulation via the thoracic duct if the SC injection site were left upper arm, whereas injections into the right upper arm, would enter either via the right thoracic duct or thoracic lymph duct (Figure 3). After abdominal SC injection, the TP would generally travel via inguinal, iliac, and lumbar LNs towards the cisterna chyli and thoracic duct, to enter the systemic blood circulation via the subclavian vein. The known anatomical structure of lymphatic system was utilized to define the sequential transfer of mAbs (24-27).

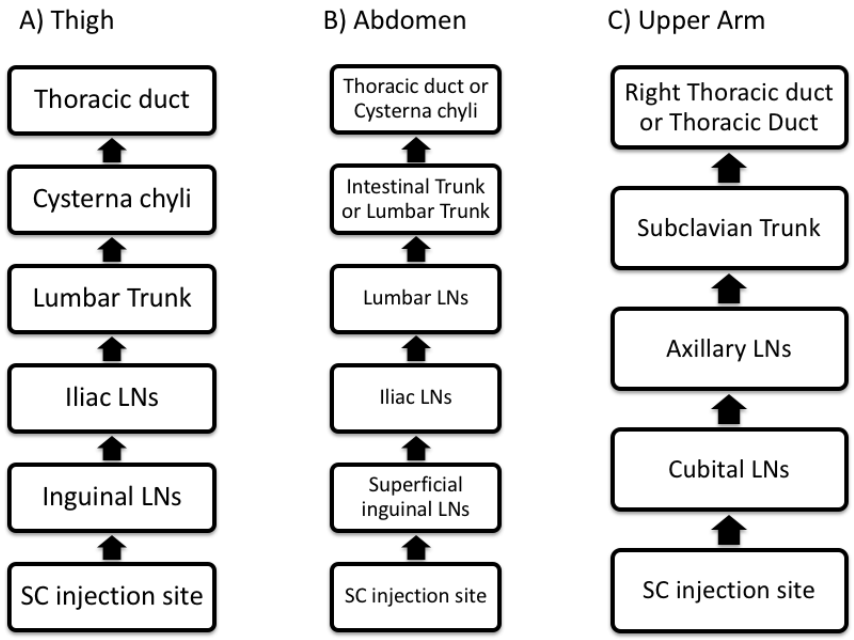

Figure 3: Sequential transfer of mAbs towards the systemic circulation after SC injection at, A) Thigh, B) Abdomen, and C) Upper Arm

The lymphatic trunk and LN volumes were combined to calculate the interstitial lymphatic trunk-LN volume. The total endosomal volume of LNs was calculated based on the endosomal volume in a peripheral mononuclear cell (28) and the number of lymphocytes in a LN (29). The endosomal LN volume and the combined lymphatic trunk-LN interstitial volume for various SC injection sites (thigh, abdomen, and upper arm) were approximately similar (Table 1).

The central lymphatic system's volume was dependent on the site of SC injection. In the case of SC injection to the thigh, abdomen or left upper arm, the TP would travel through the thoracic lymph duct. In the case of thigh and abdominal injections, volume of the cisterna chyli should be included in the central lymphatic volume. For this model, it was assumed that the SC injection site was either thigh or abdomen, therefore, the volume of the thoracic duct and cisterna chyli were included in the central lymphatic volume. However, the volume of the central lymphatic system after injection in an upper arm or thigh was found to be similar, because the volume of the cisterna chyli was negligible as compared to the thoracic duct volume (Table 1). Volumes of the thoracic lymph duct and cisterna chyli were calculated based on literature values of length and diameter. In the case of the thoracic lymph duct, the length and diameter were 45 and 5 cm,

respectively. While, in the case of cisterna chyli, the length and diameter were 2-5 mm and 1 cm, respectively (30).

Table 1: Human physiological parameters related to the SC injection site and lymphatic system		
Parameter	Value	Reference
V_{SC}^{I} (SC injection site interstitial volume)	0.003115 L	(9)
V_{SC}^{E} (SC injection site endosomal volume)	0.000025 L	(9)
V_{SC}^{V} (SC injection site vascular volume)	0.00025 L	(9)
V^{LCap} (Volume of the lymphatic capillaries)	0.00033 L	Calculated (18-20)
V_{LY-UA}^{I} (Combined interstitial volume of lymphatic trunk and LNs after SC injection in upper arm)[a]	0.01408 L	Calculated (24-27)
V_{LY}^{I} (Combined interstitial volume of lymphatic trunk and LNs after SC injection in thigh)	0.01349 L	Calculated (25-27, 31)
V_{LY-Ab}^{I} (Combined interstitial volume of lymphatic trunk and LNs after SC injection in abdomen)[a]	0.01758 L	Calculated (25-27, 32)
V_{LY-UA}^{E} (Combined endosomal volume of all LNs to which the mAb is exposed after SC injection in upper arm)[a]	0.000014 mL	Calculated (24-29)
V_{LY}^{E} (Combined endosomal volume of all LNs to which the mAb is exposed after SC injection in thigh)	0.0000126 mL	Calculated (28, 29, 31)
V_{LY-Ab}^{E} (Combined endosomal volume of all LNs to which the mAb is exposed after SC injection in abdomen)	0.00001596 mL	Calculated (25-29, 32)
V_{LY-Cen} (Volume of central lymphatic system)	0.00888 L	Calculated (30)
V_{Thor} (Volume of thoracic lymph duct)[b]	0.00884 L	Calculated (30)
V_{CC} (Volume of cisterna chyli)[b]	0.000039 L	Calculated (30)
L_{SC} (Lymph flow at the SC injection site)	0.0001356 L/h	(9)
L_{Aff} (Lymph flow afferent to LNs in human)	0.00000564 L/h	Calculated (21, 22)
L_{Eff} (Lymph flow efferent to LNs in sheep)	0.00387 L/h	(23)
L_{Thor} (Thoracic duct lymph flow rate)	0.06 L/h	(33, 34)
Q_{SC} (Blood flow at the SC injection site)	0.04992 L/h	(9)
C_{Endo} (Concentration of endogenous mAb in endosomal compartment)	10000 mg/L	(3)
Kd (Dissociation constant for antibody FcRn binding)	45.36 mg/L	(35)
nPt (FcRn concentration in SC tissue or LNs)	2880 mg/L	(36)
[a]*Not used in the model (SC injection site was assumed as thigh)* [b]*Used to calculate total central lymphatic volume*		

Table 2: mAb related parameters used in the minimal PBPK model		
Parameter	**Value**	**Reference**
σ_V (Vascular reflection coefficient)	0.95	(3, 17)
σ_L (Lymphatic reflection coefficient)	0.2	(3, 17)

$R1$ (Endosomal uptake rate of antibody)	0.00000926 /h	(3, 4)
$R2$ (Endosomal return rate of antibody)	0.26 /h	(3, 4)
FR (Recycling fraction of FcRn bound mAb)	0.715	(3)
$CL_{Endo-SC}$ (Endosomal clearance of mAb in SC injection site)[a]	0.003675 L/h	(17)
$CL_{Endo-LY}$ (Endosomal clearance of antibody in LNs)[b]	0.0001254 L/h	(17)
[a]*Endosomal clearance in skin assumed to be similar to SC injection site* [b]*Endosomal clearance in spleen assumed to be similar to lymphatic trunk-LN*		

Parameter estimation and sensitivity analysis

A nonlinear mixed-effects model with stochastic EM algorithm was used for estimation of the 2-compatmental IV PK parameters. The lymphatic trunk-LN clearance was estimated using either the nonlinear mixed-effects model with stochastic EM algorithm or a nonlinear least squares solver. Sensitivity analysis was performed on the physiological, mAb related and estimated parameters (Supplementary Figure 1 and 2). The parameters were altered by 0.1-, 0.3-, 0.5-, 0.7-, 1-, 3-, 5-, 7-, 10-, 50- and 100-fold of the original values as mentioned in Table 1. The lymphatic reflection coefficient was altered by 0.1-, 0.3-, 0.5-, 0.7-, 1-, 1.5-, 2-, 2.5-, 3-, 3.5-, 4-, 4.5-, 5- folds of the original parameter value and its impact on the PK of mAbs was determined.

Model validation

The model was validated by comparing observed and predicted PK profiles after SC administration. In addition, accuracy of the predictions was assessed by plotting ratios of $T_{max\text{-}observed}/T_{max\text{-}predicted}$, $C_{max\text{-}observed}/C_{max\text{-}predicted}$ with the *pI*, lymphatic trunk-LN clearance, and bioavailability (Supplementary Figure 3, 4 and 5). The bioavailability and *pI* values for mAbs were obtained from the literature (37-50). In the case of anifrolumab, the *pI* value was estimated using the amino acid sequence (51) and ProtParam, a web-based tool (52).

RESULTS

Estimation of the 2-compartment IV parameters

The 2-compartment model was used to estimate the parameters using the literature PK data after IV bolus or infusion (Table 3). These parameters were different for each mAb, and they were fixed in the minimal PBPK model. The mAbs had average volume of 3.5571 L (standard deviation, ± 1.1081) for the central compartment and 1.8069 L (standard deviation, ± 1.0308) for the peripheral compartment. Mean values for CL_{cen}, K_{12} and K_{21} were 0.01531 L/h, 0.0992 /h and 0.3448 /h, respectively.

Table 3: The 2-compartmental model parameters for various mAbs after IV administration

mAb	V_{cen} **(L)**	V_{per} **(L)**	CL_{cen} **(L/h)**	K_{12} **(/h)**	K_{21} **(/h)**	**Reference**
Adalimumab	3.2131	2.2382	0.01023	0.01162	0.01669	(53)
Anifrolumab	2.1732	3.7869	0.0111	0.02024	0.01161	(54)
Belimumab	3.0486	2.3877	0.009602	0.01635	0.0208	(43, 44)
Canakinumab	3.2897	2.3638	0.007541	0.009417	0.0131	(40)
Daclizumab	5.5255	1.762	0.01104	0.00257	0.00805	(55)
Golimumab	2.3293	2.3279	0.01467	0.01302	0.01302	(42, 56)
Guselkumab	4.9381	0.4131	0.0233	0.000871	0.0104	(46)
Infliximab	4.5782	1.2645	0.0169	0.8914	3.2276	(57)
Tocilizumab	3.5145	1.0064	0.03585	0.01084	0.0378	(58)
Trastuzumab	2.9608	0.5186	0.01291	0.0157	0.0896	(59, 60)
Mean	3.5571	1.8069	0.01531	0.0992	0.3448	
Standard deviation	1.1081	1.0308	0.00849	0.2784	1.0131	

Estimation of the lymphatic trunk-LN clearance

A single parameter (lymphatic trunk-LN clearance) was estimated and the rest of the model was fixed using literature values as described in the methods section. The clearance represents proteolysis of mAbs in the interstitial space of the lymphatic trunks and LNs (Figure 4). The model predicted a total of 37 SC PK profiles (10 mAbs with 26 different doses), which were compared with the mean observed published data (Figure 5 and 6). However, in the case of belimumab, the patient-PK profile was a geometric mean. The estimated lymphatic trunk-LN clearance was in the range of 0.0001495 to 0.007776 L/h with a mean of

0.00213 L/h (0.001332 to 0.002928, lower and upper 95% confidence intervals of the mean) for a total of 37 SC PK profiles. Average lymphatic trunk-LN clearance values for each mAb are shown in Table 4.

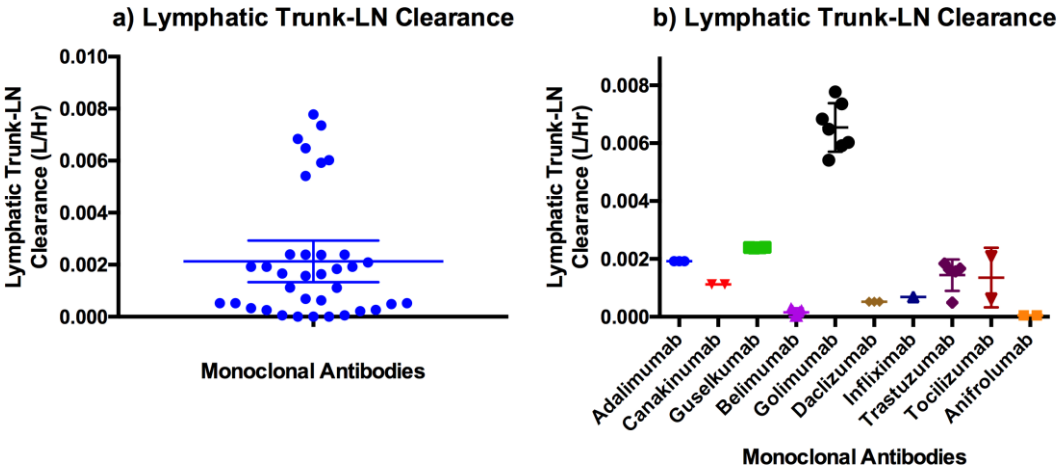

Figure 4: Estimated lymphatic trunk-LN clearance for a) all mAbs used in this study, b) individual mAbs (Mean with 95% confidence interval)

Table 4: Estimation of lymphatic trunk-LN clearance after SC administration of mAbs

mAb (SC injection site)	**SC Dose and (F)**	**Population**	**Ref.**	**Model estimated average CL_{LN}**
Adalimumab (Lower abdomen)	40 mg (64%)	Healthy volunteers	(39)	0.00192 L/h
Anifrolumab (Abdomen)	300, 600 mg (73%)	Healthy volunteers	(45)	0.00005105 L/h
Belimumab* (Abdomen or thigh)	200, 2*120, 240 mg (76%)	Lupus erythromatosus patients	(43)	0.0002564 L/h
Belimumab (Abdomen or thigh)	200, 2*120, 240 mg (76%)	Healthy volunteers	(44)	0.00000024 L/h
Canakinumab (NA)	150, 300 mg (70 %)	Healthy volunteers	(40)	0.001116 L/h
Daclizumab** (NA)	50, 150, 300 mg	Healthy volunteers	(55)	0.0005207 L/h
Golimumab (Abdomen/Thigh/Upper Arm)	50, 100 mg (50 %)	Healthy volunteers	(41, 42)	0.00651L/h
Guselkumab (NA)	10, 30, 100, 300 mg (49%)	Healthy volunteers	(46, 47)	0.002389 L/h

Infliximab (NA)	100 mg (on day 0, 28 and 56) (71%)	Rheumatoid arthritis patients	(61, 62)	0.0006855 L/h[a]
Tocilizumab (Abdomen)	162 mg (49%)	Healthy volunteers	(58)	0.002085 L/h[a]
Tocilizumab (Thigh)	162 mg (with hyaluronidase)	Healthy volunteers	(63)	0.0006258 L/h[a,b]
Trastuzumab (Thigh)	482, 645, and 776 mg (with hyaluronidase)	Healthy volunteers	(64)	0.001621 L/ h[a,c]
Trastuzumab (Thigh)	895 mg (with hyaluronidase)	HER2-positive breast cancer patients	(64)	0.0004889 L/h[a,d]
Trastuzumab (Thigh)	600 mg (with hyaluronidase)	Healthy volunteers	(65)	0.001839 L/h[a,e]
Mean CL_{LN}: 0.00213 L/h (Standard deviation: 0.002359, lower 95% confidence interval of the mean: 0.001332, upper 95% confidence interval of the mean: 0.002928 L/h)				
Nonlinear mixed-effects model with stochastic EM algorithm used for estimation of the parameters unless indicated. All observed SC PK data were mean values unless indicated. [a]*Nonlinear least squares solver* [b]SC Site lymph flow (0.04474 L/h) and CL_{LN} estimated simultaneously [c]SC Site lymph flow (0.002798 L/h) and CL_{LN} estimated simultaneously [d]SC Site lymph flow (0.003112 L/h) and CL_{LN} estimated simultaneously [e]SC Site lymph flow (0.01307 L/h) and CL_{LN} estimated simultaneously F: Bioavailability after SC administration *Geometric mean of the observed pharmacokinetic data **The model simulated median pharmacokinetic data CL_{LN}: Clearance of mAb in the lymphatic trunk-LN interstitial compartment NA: Not available				

Applications of the minimal PBPK model to evaluate impact of hyaluronidase in the mAb formulation

The mAbs for the SC administration are formulated as highly concentrated solutions in order to deliver higher doses (typically 500-900 mg). The injection volume cannot be increased more than 1-2 mL due to injection discomfort (66). However, hyaluronidase has been used in several studies to allow higher injection volumes by disrupting the complex network of the SC extracellular matrix formed by hyaluronic acid. In addition, the hyaluronidase enzyme can increase the rate of TP absorption leading to decreased T_{max}, increased C_{max}, increased area under the curve (AUC), and enhanced bioavailability of the TPs (66, 67). In this study, the SC PK data obtained after co-formulation of hyaluronidase, and tocilizumab and trastuzumab

were used to estimate the lymphatic trunk-LN clearance (58, 63-65). Due to the co-formulation with hyaluronidase, T_{max} was over-predicted for tocilizumab and trastuzumab. The *Observed* T_{max}/*Predicted* T_{max} ratio for tocilizumab and trastuzumab was 0.58 and 0.6, respectively. We hypothesized that the alteration of SC injection site by hyaluronidase may lead to altered SC injection site lymph flow. Therefore, lymphatic trunk-LN clearance and SC injection site lymph flow were estimated simultaneously (Table 4). After the simultaneous estimation of both the parameters, T_{max} prediction was improved for tocilizumab (*Observed* T_{max}/*Predicted* T_{max}= 0.87). Similarly, trastuzumab T_{max} prediction accuracy was also improved (*Observed* T_{max}/*Predicted* T_{max}= 0.82). The estimated SC injection site lymph flow for the co-formulation of the mAb and hyaluronidase was higher when compared to the original lymph flow used in the model. The estimated SC injection site lymph flow for tocilizumab was 0.04474 L/h, which was 330-fold higher than the minimal PBPK model's value (Table 1). In the case of trastuzumab, the average SC injection site lymph flow was 0.002955 L/h (22-fold higher than the original value) for healthy volunteers and HER2-positive breast cancer patients (64) (observed and model estimated PK profiles shown in Figure 6). In the case of other SC PK profile (65) (data not shown) obtained from the healthy volunteers, SC site lymph flow was 0.01307 L/h (96-fold higher than the original value).

In addition to above analysis, the SC PK (tocilizumab) profiles obtained without co-formulation with hyaluronidase enzyme were also used for simultaneous estimation of the SC injection site lymph flow and lymphatic trunk-LN clearance using the minimal PBPK model. This was done to demonstrate that the change in the SC site lymph flow observed previously was in fact due to co-formulation of hyaluronidase and mAbs. In the case of tocilizumab without hyaluronidase, the SC site lymph flow was 0.0009557 L/h (only 7-fold higher than the original value). This proves that the SC injection site lymph flow was altered when hyaluronidase co-formulation strategy was used. For the SC profiles where this strategy was not used, the SC injection site lymph flow was relatively less affected.

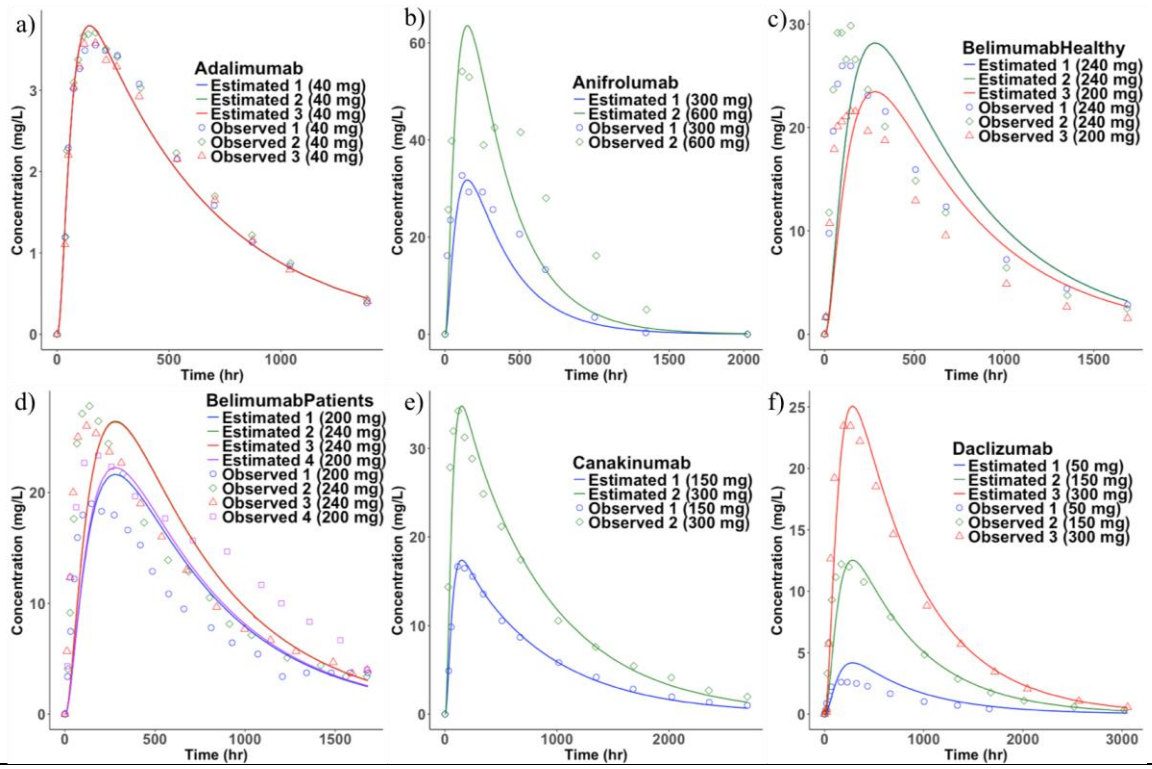

Figure 5: Observed and the model fitted SC PK profiles. a) adalimumab, b) anifrolumab, c) belimumab-Healthy, d) belimumab-patients, e) canakinumab, and f) daclizumab (Mean observed PK profiles were used for comparison with the model estimates. Observed belimumab-patient PK profile was geometric mean)

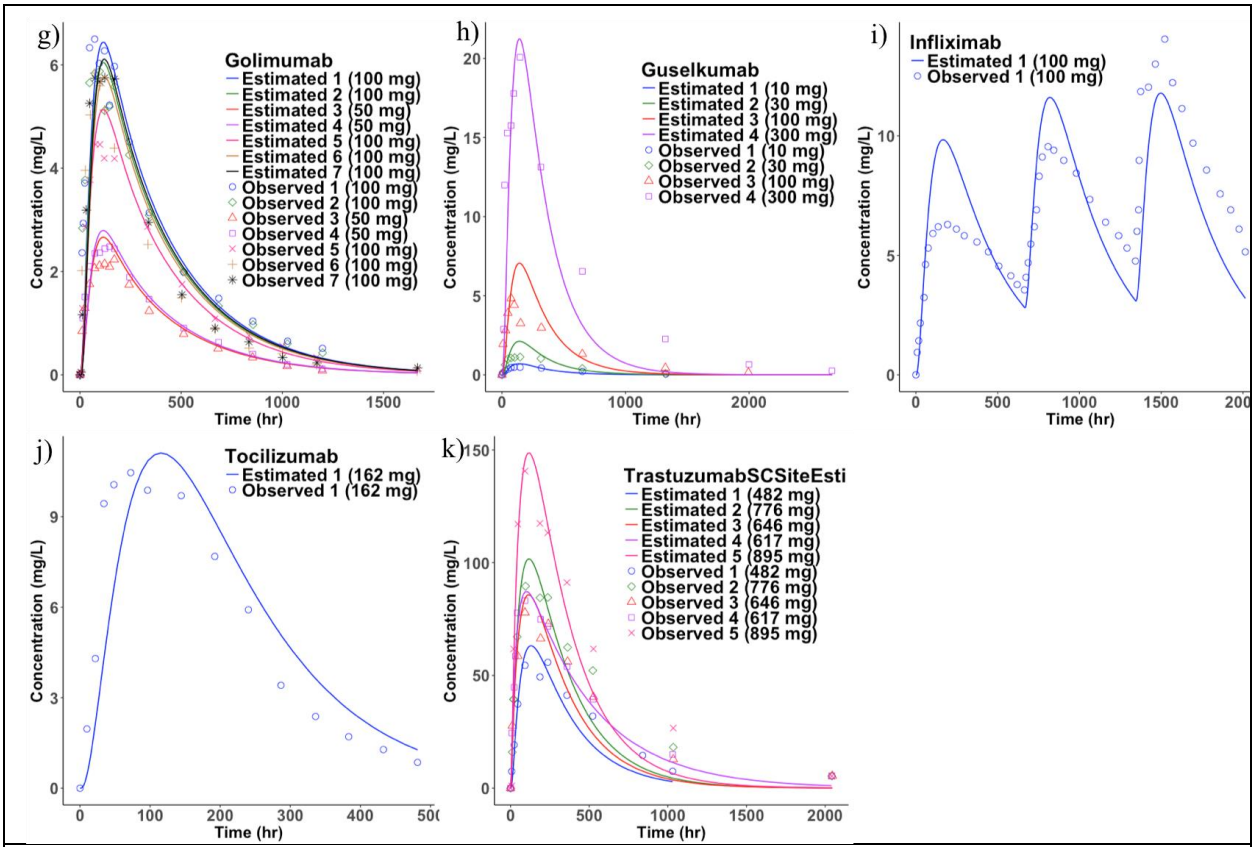

Figure 6: Observed and the model fitted SC PK profiles. g) golimumab, h) guselkumab, i) infliximab, j) tocilizumab, and k) trastuzumab (Mean observed PK profiles were used for comparison with the model estimates)

Comparison of lymphatic trunk-LN clearance with *pI* and bioavailability of mAbs

The estimated lymphatic trunk-LN clearance was compared with the *pI* (Figure 7) and bioavailability (Figure 8) of mAbs. The interstitial space has overall anionic charge due to cell surface of various immune cells in the LNs. The mAbs with higher *pI* had higher values of the estimated lymphatic trunk-LN clearance. The lymphatic trunk-LN clearance increased with decrease in bioavailability (obtained from literature) of the mAbs (Figure 8). This suggests that the model accounted for the lymphatic proteolysis of mAbs after SC administration. This may indicate that the lymphatic system was an important organ for clearance of mAbs.

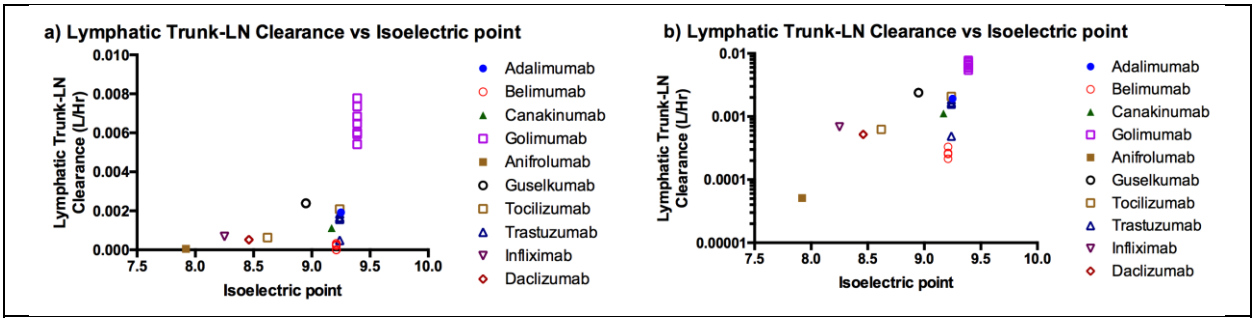

Figure 7: Correlation of the model estimated lymphatic trunk-LN clearance with the isoelectric point a) Linear scale, b) Logarithmic scale

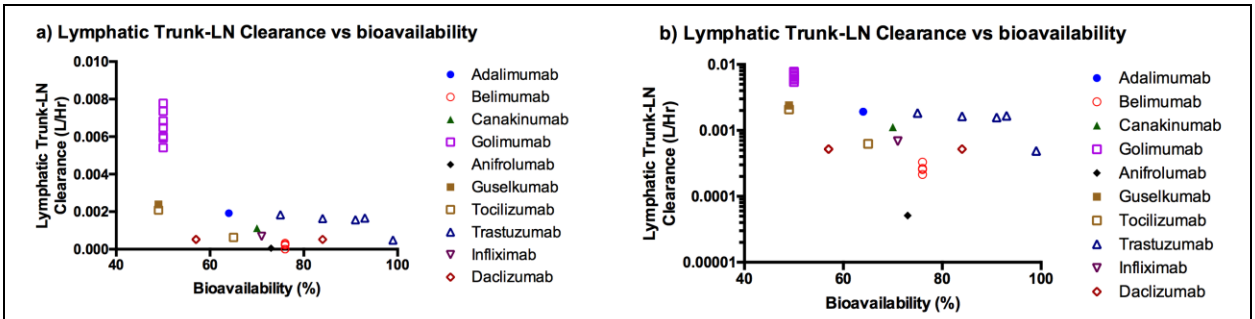

Figure 8: Correlation of the model estimated lymphatic trunk-LN clearance with the bioavailability a) Linear scale, b) Logarithmic scale (Trastuzumab: Co-formulated with hyaluronidase. Tocilizumab: Only one sample co-formulated with hyaluronidase.)

Sensitivity analysis

The sensitivity analysis showed that the SC injection site interstitial volume (V_{SC}^{I}), SC lymph flow (L_{SC}), and lymphatic capillary volume (V^{LCap}), and afferent lymph flow (L_{Aff}) were responsible for changes in C_{max} and T_{max} of mAbs (Supplementary Figure 1). In the case of lymphatic trunk-LN interstitial volume (V_{LY}^{I}), increases of the volume by 50- and 100-fold lead to alterations of mAb PK profiles, while changes by 0.1 to 10-fold of the original value did not alter C_{max} or T_{max}. The alteration of lymphatic trunk-LN clearance (CL_{LN}) and efferent lymph flow (L_{Eff}) mainly lead to modification of the C_{max}. In addition, changes in the thoracic duct lymph flow (L_{Thor}) and central lymphatic volume (V_{LY-Cen}) did not impact PK of mAbs. This indicates that transit through the initial lymphatic system after SC injection is the rate

determining step for mAb absorption instead of the thoracic duct. Therefore, SC injection site volume, SC injection site lymph flow, lymphatic capillary volume, afferent lymph flow, and efferent lymph flow are important physiological parameters for absorption of mAbs. Change in the thoracic duct lymph flow and central lymphatic volume did not alter the PK of mAbs (Supplementary Figures 1). Both the C_{max} and T_{max} were sensitive to change in the SC injection site volume, SC injection site lymph flow, lymphatic capillary volume, and afferent lymph flow (Supplementary Figures 3 to 7). However, changes in the efferent lymph flow had no impact on T_{max}. In addition, when the lymphatic reflection coefficient was increased; C_{max} decreased, while T_{max} increased. There was no change in the PK profile after alteration of the vascular reflection coefficient (Supplementary Figure 2).

Model validation

Accuracy of the model prediction was evaluated by plotting observed and predicted values of C_{max} and T_{max} (Supplementary Figure 8). In addition, the ratio of observed and predicted C_{max} and T_{max} were plotted with the *pI*, lymphatic trunk-LN clearance, and bioavailability (Supplementary Figure 9, 10, and 11). In the case of C_{max}, all predicted values were within 1.2-to 0.5-fold of the observed literature values. The predicted T_{max} was within the range of 1.8 to 0.3-fold of the observed values.

DISCUSSION

In this manuscript, the sequential transfer of mAbs after SC administration via the lymphatic system is described using the minimal PBPK model. The SC injection site (interstitial, endosomal, vascular), lymphatic capillaries, lymphatic trunk-LNs (interstitial and endosomal), central lymphatic system (thoracic duct and cisterna chyli) compartments were used to describe the transit of mAbs after SC administration. The rest of the body was modeled with a 2-compartment model based on the literature IV PK data. The sequential transfer was based on the known anatomy of lymphatic system (24-27). However, detailed routes of TP transfer via different LNs remain to be investigated further. Also, some individuals may have alterations in the clearance patterns, for example the clearance in the arm, shoulder and thigh may be

significantly changed after radical mastoidectomy. In addition, an injection site may clear into multiple adjacent lymph basins.

The clearance from the interstitial space of the SC injection site was not considered in the model, because a previously reported study indicated that protein (hGH) degradation was minimal at the SC injection site (5). In addition, simultaneous estimation of the clearance from the SC interstitial space and lymphatic trunk-LN interstitial compartment resulted in a minor contribution for the SC injection site proteolysis (data not shown). However, the endosomal proteolysis in the SC injection site and LNs was considered. The lymphatic trunk-LN interstitial clearance was estimated using the minimal PBPK model and the literature SC PK data (Figure 4 and Table 4). The estimated clearance differed with dosing and population changes. This alteration of the estimated clearance may be due to disease condition, change in formulation, or the differences in posttranslational modifications (e.g. glycosylation). These differences were not considered in the model. The model demonstrated that the estimated lymphatic trunk-LN clearance of mAbs may correlate with the bioavailability (Figure 8). The estimated clearance increased when the bioavailability of the mAb decreased. This indicates efficiency of the model to account for the proteolysis of mAbs in the lymphatic system. According to the previously published reports, proteolysis was not observed after incubation of TPs with the freshly collected lymph, indicating absence of any protease enzymes in the lymph (5, 68). In this study, the lymphatic trunk volume (which mainly contains lymph fluid) and the LN (which mainly contains lymph node cells) volume were combined to represent the compartment responsible for proteolysis of the mAbs. The lymphatic trunk-LN compartment was mainly composed of the LN volume. The lymphatic trunk volume representing volume of the lymph fluid was very minor (< 7%).

Sensitivity analysis (Supplementary Figure 1) showed that the lymphatic trunk-LN interstitial space proteolysis was important to govern C_{max} of the mAbs. The degradation of mAbs in the lymphatic system was primarily due to extracellular or interstitial proteolysis. The protease enzymes secreted by the LN and other immune cells in the interstitial space may play an important role in reducing the bioavailability of mAbs. Intracellular or endosomal proteolysis of mAbs was negligible due to FcRn binding-mediated

protection. The intracellular proteolysis of mAbs in the lymphatic system may be dependent on their uptake by the lymphocytes. In this model, we used endosomal uptake rate (R1) from a literature PBPK model (estimated by fitting liver data) (3, 4). Alteration of the endosomal uptake rate by 0.1 to 100-fold of the original value did not change the PK of mAbs (data not shown). However, *in vitro* studies to calculate R1 may be useful for an accurate understanding of proteolytic processes in the SC injection site and lymphatic system. Disease conditions like inflammation may also increase proteolytic activity of the lymph. However, this remains to be further investigated. Further, alteration of the recycling fraction of FcRn bound mAb, dissociation constant for antibody FcRn binding, and FcRn concentration did not change PK of mAbs (data not shown).

Wang et al. (68) confirmed proteolysis of erythropoietin in the presence of rat LN cell suspension. When number of LN cells in the incubation was increased, the protein completely disappeared. This indicates that LNs are responsible for proteolysis of TPs. In addition, after incubation of the protein with the SC tissue homogenate, 90-95% of the parent protein remained unaffected (68). Although the authors raised doubts about loss of proteolytic activity during preparation of the SC tissue homogenate, this finding corroborates our conclusion that the SC site degradation plays a minor role in governing the bioavailability. However, in another study, insulin was reported to degrade at the SC injection site (69). Detailed investigation of *in vitro* proteolysis of mAbs in various systems must be done to arrive at more definite conclusions about the cause of reduced bioavailability after SC administration.

The PK studies in humans indicate that variation in the injection site (abdomen and thigh) do not have any impact on C_{max} and $AUC_{0-\infty}$ of belimumab (44). In another clinical study, golimumab's median T_{max} after SC injection in the thigh was 1.25-fold higher than SC injection in the abdomen and upper arm. The C_{max} after thigh SC injection was 1.33-fold higher than SC injection in the upper arm, and the C_{max}-abdomen was 1.24-fold higher than that of the upper arm (42). This suggests that the volumes of lymphatic compartments and lymph flows may not be significantly different for each of the SC injection sites. Therefore, lymphatic volumes and flows rates for one injection site may be applied to the other. The calculations used in the

model showed that the interstitial volume of the lymphatic trunk-LN was similar for various SC injection sites (upper arm, abdomen, and thigh) (Table 1).

The prediction accuracy of the model was determined by plotting observed and predicted PK parameters (Supplementary Figure 8). There was no correlation of the prediction accuracy of T_{max} or C_{max} with the *pI* or bioavailability or the estimated lymphatic trunk-LN clearance of mAbs. This confirms that the *pI* of mAbs did not affect the uptake by lymphatic system. Similarly, lymphatic trunk-LN clearance and bioavailability did not govern the prediction accuracy of the model.

The model also showed that for the mAbs with higher *pI*, the estimated lymphatic trunk-LN clearance was greater. The cationic proteins with higher *pI* have a propensity to bind with the anionic cell surfaces and interstitial space (e.g. hyaluronic acid). Higher *pI* also leads to faster clearance of mAbs (70). Similar trend was observed for the mAbs investigated in this study (Figure 7). This correlation may be used to predict the lymphatic trunk-LN clearance based on the known *pI* of mAbs. The lymphatic clearance can be used in the minimal PBPK model to predict SC PK of the mAbs.

Sensitivity analysis of the model parameters indicated that the initial lymphatics are rate determining for absorption of mAbs via the SC route. Mainly, the SC injection site lymph flow, SC injection site volume, afferent lymph flow, efferent lymph flow, and lymphatic trunk-LN volume impacted T_{max}, after their alteration by 0.1 to 100-fold of the original value. However, thoracic duct lymph flow had no effect on T_{max} even after 0.1 to 100-fold changes in its value. The thoracic lymph duct, which is the largest lymphatic vessel, may not change the rate of transit of mAbs. Therefore, alteration of thoracic lymph duct flows due to disease condition may not alter overall PK of mAbs. However, the parameters associated with the initial lymphatic system are important to govern the absorption of mAbs and change in those parameters due to the disease conditions may significantly alter the SC PK of mAbs.

It was reported earlier that the PK of mAbs is prone to high inter-subject variability. Factors like body weight, age, sex, ethnicity, disease condition, immune status are responsible for variations in the PK (71). However, more research is needed to evaluate their influence on physiological parameters related to the SC injection site and lymphatic system. The minimal PBPK model may be used for prediction of bioavailability of mAbs using *in vitro* lymphatic proteolysis data and to evaluate the impact of changes in lymphatic flow rates on the PK. In addition, the model may be utilized to guide *in vitro* experiments for mechanistic prediction of the bioavailability. This study has explained various physiological parameters related to the SC injection site and lymphatic system responsible for regulating the PK of mAbs.

CONCLUSION

The lymphatic trunk-LN clearance was estimated using the minimal PBPK model. The physiological parameters related to the SC tissue and lymphatic system were used along with the 2-compartment IV parameters to construct the minimal PBPK model for prediction of SC PK of the mAbs. The model may serve as a platform to utilize the *in vitro* clearance data from the SC tissue and lymphatic system to predict SC PK of mAbs. The LNs were mainly responsible for proteolysis of mAbs leading to their reduced bioavailability. Therefore, LN cell suspension may be used to generate inputs for the PBPK model. However, the *in vitro* studies were beyond the scope of this manuscript. Further, this study identified SC injection site lymph flow, afferent lymph flow, efferent lymph flow, volumes associated with the SC injection site, and lymphatic trunk-LN clearance as important parameters responsible for absorption of mAbs. The lymphatic trunk-LN clearance increased with increase in the *pI* of mAbs. Therefore, the *pI* of mAbs can be used to calculate the lymphatic clearance. Overall, the model is useful to understand disposition of mAbs after SC administration.

ACKNOWLEDGEMENT

The authors were supported by a generous grant from NIH (R01CA173292). NV was partially supported by a Higuchi Fellowship and the Department of Pharmaceutical Chemistry, The University of Kansas. We are also grateful to the J.R. and Inez Jay funds, awarded to MLF by the Higuchi Biosciences Center at The University of Kansas.

APPENDIX

In addition to the data figures in the Supplementary materials, all raw digitalized data and the SimBiology (Matlab 2017a) model file used in this study are archived and available free of charge at the University of Kansas ScholarWorks Repository (https://kuscholarworks.ku.edu/handle/ *repository ID pending manuscript acceptance*).

Model equations

$$V_{SC}^{I}\left(\frac{dC_{SC}^{I}}{dt}\right) = \left((1-\sigma_V)\times L_{SC}\times C_{SC}^{V}\right) - (R1\times C_{SC}^{I}) + \left((1-FR)\times R2\times(1-f_{uSC})\times C_{SC}^{E}\right) - \left((1-\sigma_L)\times L_{SC}\times C_{SC}^{I}\right)$$

$$V_{SC}^{V}\left(\frac{dC_{SC}^{V}}{dt}\right) = -\left((1-\sigma_V)\times L_{SC}\times C_{SC}^{V}\right) - \left((Q_{SC}-L_{SC})\times C_{SC}^{V}\right) + (FR\times R2\times(1-f_{uSC})\times C_{SC}^{E}) - \left(R1\times C_{SC}^{V}\right) + (Q_{SC}\times C_{Cen})$$

$$V_{SC}^{E}\left(\frac{dC_{SC}^{E}}{dt}\right) = (R1\times C_{SC}^{I}) - (FR\times R2\times(1-f_{uSC})\times C_{SC}^{E}) - \left((1-FR)\times R2\times(1-f_{uSC})\times C_{SC}^{E}\right) + \left(R1\times C_{SC}^{V}\right) - ((1-f_{uSC})\times CL_{Endo-SC}\times C_{SC}^{E})$$

$$V^{LCap}\left(\frac{dC^{LCap}}{dt}\right) = \left((1-\sigma_L)\times L_{SC}\times C^{LCap}\right) - \left(L_{Aff}\times C^{LCap}\right)$$

$$V_{LN}^{I}\left(\frac{dC_{LN}^{I}}{dt}\right) = \left(L_{Aff}\times C_{LN}^{Cap}\right) - \left(L_{Eff}\times C_{LN}^{I}\right) - (CL_{LN}\times C_{LN}^{I}) - (R1\times C_{LN}^{I}) + \left((1-FR)\times R2\times(1-f_{uLN})\times C_{LN}^{E}\right)$$

$$V_{LN}^{E}\left(\frac{dC_{LN}^{E}}{dt}\right) = (R1 \times C_{LN}^{I}) - \left((1 - FR) \times R2 \times (1 - f_{uLN}) \times C_{LN}^{E}\right) - ((1 - f_{uLN}) \times CL_{Endo-LN} \times C_{LN}^{E})$$

$$V_{LN-Cen}\left(\frac{dC_{LN-Cen}}{dt}\right) = -(L_{Thor} \times C_{LN-Cen}) + \left(L_{Eff} \times C_{LN}^{I}\right)$$

$$V_{Cen}\left(\frac{dC_{Cen}}{dt}\right) = (L_{Thor} \times C_{LN-Cen}) + ((Q_{SC} - L_{SC}) \times C_{SC}^{V}) - (CL_{Cen} \times C_{Cen}) - (K_{12} \times C_{Cen}) + (K_{21} \times C_{Per}) - (Q_{SC} \times C_{Cen})$$

$$V_{Per}\left(\frac{dC_{Per}}{dt}\right) = (K_{12} \times C_{Cen}) - (K_{21} \times C_{Per})$$

$$f_{uSC} = 1 - \left(\frac{1}{2 \times (C_{Endo} + C_{SC}^{E})}\right) \times \left((K_d + nPt + C_{Endo} + C_{SC}^{E}) - \left(\sqrt{(Kd + nPt + C_{Endo} + C_{SC}^{E})^2 - (4 \times (C_{Endo} + C_{SC}^{E}) \times nPt)}\right)\right)$$

$$f_{uLN} = 1 - \left(\frac{1}{2 \times (C_{Endo} + C_{LN}^{E})}\right) \times \left((K_d + nPt + C_{Endo} + C_{LN}^{E}) - \left(\sqrt{(Kd + nPt + C_{Endo} + C_{LN}^{E})^2 - (4 \times (C_{Endo} + C_{LN}^{E}) \times nPt)}\right)\right)$$

Glossary

Parameter	Definition
C_{SC}^{V}	Concentration of mAb in the vascular space of SC injection site
C_{SC}^{I}	Concentration of mAb in the interstitial space of SC injection site
C_{SC}^{E}	Concentration of mAb in the endosomal space of SC injection site
C^{LCap}	Concentration of mAb in the lymphatic capillary compartment
C_{LN}^{I}	Concentration of mAb in the interstitial space of lymphatic trunk-LNs
C_{LN}^{E}	Concentration of mAb in the endosomal space of lymphatic trunk-LNs
C_{LY-Cen}	Concentration of mAb in the central lymphatic system
C_{Cen}	Concentration of mAb in the central compartment
C_{Per}	Concentration of mAb in the peripheral compartment
V_{SC}^{I}	SC injection site interstitial volume

V_{SC}^{V}	SC injection site vascular volume
V_{SC}^{E}	SC injection site endosomal volume
V^{LCap}	Volume of the lymphatic capillaries
V_{LN}^{I}	Combined interstitial volume of lymphatic trunk-LNs after SC injection in thigh
V_{LN}^{E}	Combined endosomal volume of all LNs to which the mAb is exposed after SC injection in thigh
V_{LY-Cen}	Volume of central lymphatic system
V_{Cen}	Volume of the central compartment
V_{Per}	Volume of the peripheral compartment
L_{SC}	Lymph flow at the SC injection site
L_{Aff}	Lymph flow afferent to LNs
L_{Eff}	Lymph flow efferent to LNs
L_{Thor}	Thoracic duct lymph flow
Q_{SC}	Blood flow at the SC injection site
σ_L	Lymphatic reflection coefficient
σ_V	Vascular reflection coefficient
CL_{LN}	Clearance of mAb in the lymphatic trunk-LN interstitial compartment
$CL_{Endo-SC}$	Endosomal clearance of mAb in the SC injection site
$CL_{Endo-LN}$	Endosomal clearance of mAb in LNs
CL_{Cen}	Clearance of mAb from the central compartment
K_{12}	Transfer rate constant from the central compartment to the peripheral compartment
K_{21}	Transfer rate constant from the peripheral compartment to the central compartment
f_{uSC}	Unbound fraction of mAb in SC tissue
f_{uLN}	Unbound fraction of mAb in lymphatic trunk and LNs
C_{Endo}	Concentration of endogenous mAb in endosomal compartment
$R1$	Endosomal uptake rate of antibody
$R2$	Endosomal return rate of antibody
FR	Recycling fraction of FcRn bound mAb
Kd	Dissociation constant for antibody FcRn binding
nPt	*FcRn concentration in SC tissue or LN*

REFERENCES

1. Jackisch C, Müller V, Maintz C, Hell S, Ataseven B. Subcutaneous administration of monoclonal antibodies in oncology. Geburtshilfe Frauenheilkd. 2014;74(4):343
2. Dirks NL, Meibohm B. Population pharmacokinetics of therapeutic monoclonal antibodies. Clin Pharmacokinet. 2010;49(10):633-659
3. Zhao L, Ji P, Li Z, Roy P, Sahajwalla CG. The antibody drug absorption following subcutaneous or intramuscular administration and its mathematical description by coupling physiologically based absorption process with the conventional compartment pharmacokinetic model. J Clin Pharmacol. 2013;53(3):314-325
4. Davda JP, Jain M, Batra SK, Gwilt PR, Robinson DH. A physiologically based pharmacokinetic (PBPK) model to characterize and predict the disposition of monoclonal

antibody CC49 and its single chain Fv constructs. Int Immunopharmacol. 2008;8(3):401-413
5. Charman SA, Segrave AM, Edwards GA, Porter CJ. Systemic availability and lymphatic transport of human growth hormone administered by subcutaneous injection. J Pharm Sci. 2000;89(2):168-177
6. Abuqayyas L, Balthasar JP. Application of PBPK modeling to predict monoclonal antibody disposition in plasma and tissues in mouse models of human colorectal cancer. J Pharmacokinet Pharmacodyn. 2012;39(6):683-710
7. Baxter LT, Zhu H, Mackensen DG, Butler WF, Jain RK. Biodistribution of monoclonal antibodies: scale-up from mouse to human using a physiologically based pharmacokinetic model. Cancer Res. 1995;55(20):4611-4622
8. Shah DK, Betts AM. Towards a platform PBPK model to characterize the plasma and tissue disposition of monoclonal antibodies in preclinical species and human. J Pharmacokinet Pharmacodyn. 2012;39(1):67-86
9. Gill KL, Gardner I, Li L, Jamei M. A bottom-up whole-body physiologically based pharmacokinetic model to mechanistically predict tissue distribution and the rate of subcutaneous absorption of therapeutic proteins. AAPS J. 2016;18(1):156-170
10. Chen X, DuBois DC, Almon RR, Jusko WJ. Interrelationships between Infliximab and rhTNF-α in Plasma using Minimal Physiologically-Based Pharmacokinetic (mPBPK) Models. Drug Metab Dispos. 2017;45(7):790-797
11. Elmeliegy M, Lowe P, Krzyzanski W. Simplification of complex physiologically based pharmacokinetic models of monoclonal antibodies. AAPS J. 2014;16(4):810-842
12. Li L, Gardner I, Dostalek M, Jamei M. Simulation of Monoclonal Antibody Pharmacokinetics in HumansUsing a Minimal Physiologically Based Model. AAPS J. 2014;16(5):1097-1109
13. Sager JE, Yu J, Raguenau-Majlessi I, Isoherranen N. Physiologically based pharmacokinetic (PBPK) modeling and simulation approaches: a systematic review of published models, applications and model verification. Drug Metab Dispos. 2015:dmd. 115.065920
14. Wong H, Chow TW. Physiologically based pharmacokinetic modeling of therapeutic proteins. J Pharm Sci. 2017;106(9):2270-2275
15. Rohatgi A. WebPlotDigitizer, Web based tool to extract data from plots, images, and maps. 2018 Accessed on May 09, 2018. Available from: https://automeris.io/WebPlotDigitizer/.
16. Kuo I, Akpa BS. Validity of the Lipid Sink as a Mechanism for the Reversal of Local Anesthetic Systemic ToxicityA Physiologically Based Pharmacokinetic Model Study. Anesthesiology: The Journal of the American Society of Anesthesiologists. 2013;118(6):1350-1361
17. Garg A, Balthasar JP. Physiologically-based pharmacokinetic (PBPK) model to predict IgG tissue kinetics in wild-type and FcRn-knockout mice. J Pharmacokinet Pharmacodyn. 2007;34(5):687-709
18. Mellor R, Stanton A, Azarbod P, Sherman M, Levick J, Mortimer P. Enhanced cutaneous lymphatic network in the forearms of women with postmastectomy oedema. J Vasc Res. 2000;37(6):501-512

19. Nathanson SD, Nelson L, Karvelis KC. Rates of flow of technetium 99m-labeled human serum albumin from peripheral injection sites to sentinel lymph nodes. Ann Surg Oncol. 1996;3(4):329-335
20. Margaris K, Black RA. Modelling the lymphatic system: challenges and opportunities. J R Soc Interface. 2012;9(69):601-612
21. Fischer M, Franzeck UK, Herrig I, Costanzo U, Wen S, Schiesser M, Hoffmann U, Bollinger A. Flow velocity of single lymphatic capillaries in human skin. Am J Physiol Heart Circ Physiol. 1996;270(1):H358-H363
22. Fujiwara M, Sawada M, Kasuya A, Matsushita Y, Yamada M, Fukamizu H, Magata Y, Tokura Y, Sakahara H. Measurement of cutaneous lymphatic flow rates in patients with skin cancer: area extraction method. J Dermatol. 2014;41(6):498-504
23. Quin J, Shannon A. The influence of the lymph node on the protein concentration of efferent lymph leaving the node. J Physiol. 1977;264(2):307-321
24. Lymphatics of the Upper Limb. Department of Neurobiology and Developmental Sciences, University of Arkansas for Medical Sciences. Accessed on April 14, 2018. Available from: http://anatomy.uams.edu/lymph_upperlimb.html.
25. Bontumasi N, Jacobson JA, Caoili E, Brandon C, Kim SM, Jamadar D. Inguinal lymph nodes: size, number, and other characteristics in asymptomatic patients by CT. Surg Radiol Anat. 2014;36(10):1051-1055
26. Usovich A, Borziak E. Variants in the number and size and the topography of the lumbar lymph nodes in the regional of the liver in the human adult. Arkh Anat Gistol Ehmbriol. 1982;83(7):29-33
27. Ying M, Pang B. Three-dimensional ultrasound measurement of cervical lymph node volume. Br J Radiol. 2009;82(980):617-625
28. Corlier F, Rivals I, Lagarde J, Hamelin L, Corne H, Dauphinot L, Ando K, Cossec J, Fontaine G, Dorothée G. Modifications of the endosomal compartment in peripheral blood mononuclear cells and fibroblasts from Alzheimer's disease patients. Transl Psychiatry. 2015;5(7):e595
29. Sikorski E, Gerberick G, Ryan C, Miller C, Ridder G. Phenotypic analysis of lymphocyte subpopulations in lymph nodes draining the ear following exposure to contact allergens and irritants. Fundam Appl Toxicol. 1996;34(1):25-35
30. Skandalakis JE, Skandalakis LJ, Skandalakis PN. Anatomy of the lymphatics. Surg Oncol Clin N Am. 2007;16(1):1-16
31. Lymphatics of the Lower Limb. Department of Neurobiology and Developmental Sciences, University of Arkansas for Medical Sciences. Accessed on April 14, 2018. Available from: http://anatomy.uams.edu/lymph_lowerlimb.html.
32. Lymphatics of the Abdomen. Department of Neurobiology and Developmental Sciences, University of Arkansas for Medical Sciences. Accessed on April 14, 2018. Available from: http://anatomy.uams.edu/lymph_abdomen.html.
33. Giragossian C, Vage C, Li J, Pelletier K, Piché-Nicholas N, Rajadhyaksha M, Liras J, Logan A, Calle RA, Weng Y. Mechanistic Investigation of the Preclinical Pharmacokinetics and Interspecies Scaling of PF-05231023, a Fibroblast Growth Factor 21–Antibody Protein Conjugate. Drug Metab Dispos. 2015;43(6):803-811
34. Dumont AE, Mulholland JH. Flow rate and composition of thoracic-duct lymph in patients with cirrhosis. N Engl J Med. 1960;263(10):471-474

35. Zhou J, Johnson JE, Ghetie V, Ober RJ, Ward ES. Generation of mutated variants of the human form of the MHC class I-related receptor, FcRn, with increased affinity for mouse immunoglobulin G. J Mol Biol. 2003;332(4):901-913
36. Ferl GZ, Wu AM, DiStefano JJ. A predictive model of therapeutic monoclonal antibody dynamics and regulation by the neonatal Fc receptor (FcRn). Ann Biomed Eng. 2005;33(11):1640-1652
37. Center for drug evaluation and research, guselkumab application 761061Orig1s000 2018 Accessed on April 13, 2018. Available from: https://www.accessdata.fda.gov/drugsatfda_docs/nda/2017/761061Orig1s000OtherR.pdf.
38. Doyle Keith, Halo Maria, Harding Emma R, Lewis Peter, Uden Mark, Damian Valeriu, Xuan H. Antibody variants. In.; 2017.
39. Hillson J, Mant T, Rosano M, Huntenburg C, Alai-Safar M, Darne S, Palmer D, Pavlova BG, Doralt J, Reeve R. Pharmacokinetic equivalence, comparable safety, and immunogenicity of an adalimumab biosimilar product (M923) to Humira in healthy subjects. Pharmacol Res Perspect. 2018;6(1)
40. Chakraborty A, Tannenbaum S, Rordorf C, Lowe PJ, Floch D, Gram H, Roy S. Pharmacokinetic and pharmacodynamic properties of canakinumab, a human anti-interleukin-1β monoclonal antibody. Clin Pharmacokinet. 2012;51(6):e1-e18
41. Ling J, Lyn S, Xu Z, Achira M, Bouman-Thio E, Shishido A, Ford J, Shankar G, Wagner C, Kim KT. Lack of racial differences in the pharmacokinetics of subcutaneous golimumab in healthy Japanese and Caucasian male subjects. J Clin Pharmacol. 2010;50(7):792-802
42. Xu Z, Wang Q, Zhuang Y, Frederick B, Yan H, Bouman-Thio E, Marini JC, Keen M, Snead D, Davis HM. Subcutaneous bioavailability of golimumab at 3 different injection sites in healthy subjects. J Clin Pharmacol. 2010;50(3):276-284
43. Yapa SWS, Roth D, Gordon D, Struemper H. Comparison of intravenous and subcutaneous exposure supporting dose selection of subcutaneous belimumab systemic lupus erythematosus Phase 3 program. Lupus. 2016;25(13):1448-1455
44. Cai WW, Fiscella M, Chen C, Zhong ZJ, Freimuth WW, Subich DC. Bioavailability, pharmacokinetics, and safety of belimumab administered subcutaneously in healthy subjects. Clin Pharmacol Drug Dev. 2013;2(4):349-357
45. Tummala R, Rouse T, Berglind A, Santiago L. Safety, tolerability, and pharmacokinetics of subcutaneous and intravenous anifrolumab in healthy volunteers. In.ACR/ARHP Annual Meeting: BMJ Publishing Group Ltd; 2017.
46. Zhuang Y, Calderon C, Marciniak SJ, Bouman-Thio E, Szapary P, Yang T-Y, Schantz A, Davis HM, Zhou H, Xu Z. First-in-human study to assess guselkumab (anti-IL-23 mAb) pharmacokinetics/safety in healthy subjects and patients with moderate-to-severe psoriasis. Eur J Clin Pharmacol. 2016;72(11):1303-1310
47. Product monograph for Tremfya (guselkumab). Janssen Inc. . Accessed on April 16, 2018. Available from: http://www.janssen.com/canada/sites/www_janssen_com_canada/files/prod_files/live/tremfya_cpm.pdf.
48. Infliximab DrugBank. 2018 Accessed on May 17, 2018. Available from: https://www.drugbank.ca/drugs/DB00065.

49. Daclizumab DrugBank. 2018 Accessed on May 17, 2018. Available from: https://www.drugbank.ca/drugs/DB00111.
50. Miao S, Fan L, Zhao L, Ding D, Liu X, Wang H, Tan W-S. Physicochemical and Biological Characterization of the Proposed Biosimilar Tocilizumab. Biomed Res Int. 2017;2017
51. International Nonproprietary Names for Pharmaceutical Substances (INN), WHO Drug Information, Vol. 28, No. 1, 2014 (INN List 71). Accessed on May 25, 2018. Available from: http://www.who.int/medicines/publications/druginformation/innlists/RL71.pdf.
52. Gasteiger E, Hoogland C, Gattiker A, Wilkins MR, Appel RD, Bairoch A. Protein identification and analysis tools on the ExPASy server. In. The proteomics protocols handbook: Springer; 2005. p. 571-607.
53. Weisman MH, Moreland LW, Furst DE, Weinblatt ME, Keystone EC, Paulus HE, Teoh LS, Velagapudi RB, Noertersheuser PA, Granneman GR. Efficacy, pharmacokinetic, and safety assessment of adalimumab, a fully human anti-tumor necrosis factor-alpha monoclonal antibody, in adults with rheumatoid arthritis receiving concomitant methotrexate: a pilot study. Clin Ther. 2003;25(6):1700-1721
54. Goldberg A, Geppert T, Schiopu E, Frech T, Hsu V, Simms RW, Peng SL, Yao Y, Elgeioushi N, Chang L. Dose-escalation of human anti-interferon-α receptor monoclonal antibody MEDI-546 in subjects with systemic sclerosis: a phase 1, multicenter, open label study. Arthritis Res Ther. 2014;16(1):R57
55. Othman AA, Tran JQ, Tang MT, Dutta S. Population pharmacokinetics of daclizumab high-yield process in healthy volunteers: integrated analysis of intravenous and subcutaneous, single-and multiple-dose administration. Clin Pharmacokinet. 2014;53(10):907-918
56. Zhou H, Jang H, Fleischmann RM, Bouman-Thio E, Xu Z, Marini JC, Pendley C, Jiao Q, Shankar G, Marciniak SJ. Pharmacokinetics and safety of golimumab, a fully human anti-TNF-α monoclonal antibody, in subjects with rheumatoid arthritis. J Clin Pharmacol. 2007;47(3):383-396
57. Palaparthy R, Udata C, Hua SY, Yin D, Cai C-H, Salts S, Rehman MI, McClellan J, Meng X. A randomized study comparing the pharmacokinetics of the potential biosimilar PF-06438179/GP1111 with Remicade®(infliximab) in healthy subjects (REFLECTIONS B537-01). Expert Rev Clin Immunol. 2018;14(4):329-336
58. Zhang X, Georgy A, Rowell L. Pharmacokinetics and pharmacodynamics of tocilizumab, a humanized anti-interleukin-6 receptor monoclonal antibody, following single-dose administration by subcutaneous and intravenous routes to healthy subjects. Int J Clin Pharmacol Ther. 2013;51(6):443-455
59. Morita J, Tanaka M, Nomoto M, Matsuki S, Tsuru T, Matsuguma K, Shiramoto M. Pharmacokinetic bioequivalence, safety, and immunogenicity of DMB-3111, a trastuzumab biosimilar, and trastuzumab in healthy Japanese adult males: results of a randomized trial. BioDrugs. 2016;30(1):17-25
60. Pivot X, Deslypere JP, Park LS, Kim MJ, Lee W, Lee J. A Randomized Phase I Study Comparing the Pharmacokinetics of HD201, a Trastuzumab Biosimilar, With European Union–sourced Herceptin. Clin Ther. 2018;40(3):396-405. e394
61. Westhovens R, Houssiau F, Joly J, Everitt DE, Zhu Y, Sisco D, Van Hartingsveldt B, Mascelli MA, Graham MA, Durez P. A phase I study assessing the safety, clinical response, and pharmacokinetics of an experimental infliximab formulation for

subcutaneous or intramuscular administration in patients with rheumatoid arthritis. J Rheumatol. 2006;33(5):847-853
62. Zhu Y, Pendley C, Sisco D, Westhovens R, Durez P, Bouman-Thio E, Hartingsveldt B, Everitt D, Graham M. Pharmacokinetics and pharmacodynamics of infliximab, an anti-tumor necrosis factor-alpha monoclonal antibody, following single subcutaneous administrations in rheumatoid arthritis patients. Clin Pharmacol Ther. 2005;77(2)
63. Morcos PN, Zhang X, McIntyre C, Bittner B, Rowell L, Hussain Z. Pharmacokinetics and pharmacodynamics of single subcutaneous doses of tocilizumab administered with or without rHuPH20. Int J Clin Pharmacol Ther. 2013;51(7):537-548
64. Wynne C, Harvey V, Schwabe C, Waaka D, McIntyre C, Bittner B. Comparison of Subcutaneous and Intravenous Administration of Trastuzumab: A Phase I/Ib Trial in Healthy Male Volunteers and Patients With HER2-Positive Breast Cancer. J Clin Pharmacol. 2013;53(2):192-201
65. Wynne CJ, Ellis-Pegler RB, Waaka DS, Schwabe C, Lehle M, Heinzmann D, Mangat R, Li C, Dick AE, Cranshaw NA. Comparative pharmacokinetics of subcutaneous trastuzumab administered via handheld syringe or proprietary single-use injection device in healthy males. Cancer Chemother Pharmacol. 2013;72(5):1079-1087
66. Richter WF, Jacobsen B. Subcutaneous Absorption of Biotherapeutics: Knowns and Unknowns. Drug Metab Dispos. 2014;42(11):1881-1889
67. Liu S, Xie B, Wei W, Hui M, Su Z. Design and preparation of chimeric hyaluronidase as a chaperone for the subcutaneous administration of biopharmaceuticals. Biochem Eng J. 2016;112:32-41
68. Wang W, Chen N, Shen X, Cunningham P, Fauty S, Michel K, Wang B, Hong X, Adreani C, Nunes CN. Lymphatic transport and catabolism of therapeutic proteins after subcutaneous administration to rats and dogs. Drug Metab Dispos. 2012;40(5):952-962
69. Okumura K, Komada F, Hori R. Fate of porcine and human insulin at the subcutaneous injection site. I. degradation and absorption of insulins in the rat. J Pharmacobiodyn. 1985;8(1):25-32
70. Bumbaca D, Boswell CA, Fielder PJ, Khawli LA. Physiochemical and biochemical factors influencing the pharmacokinetics of antibody therapeutics. AAPS J. 2012;14(3):554-558
71. Gill KL, Machavaram KK, Rose RH, Chetty M. Potential sources of inter-subject variability in monoclonal antibody pharmacokinetics. Clin Pharmacokinet. 2016;55(7):789-805